Electronic Supplementary Material (ESI) for Energy & Environmental Science

Supplementary Information

Direct Observation of the Reduction of Carbon Dioxide by Rhenium Bipyridine Catalysts

Matthew D. Sampson,[a] Jesse D. Froehlich,[a] Jonathan M. Smieja,[a] Eric E. Benson,[a] Ian D. Sharp,[b,c] and Clifford P. Kubiak*[a]

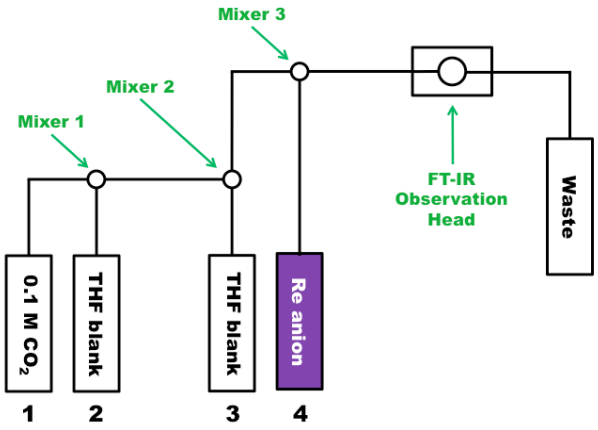

Fig. S1. Mixing schematic for a typical stopped-flow IR spectroscopy experiment.

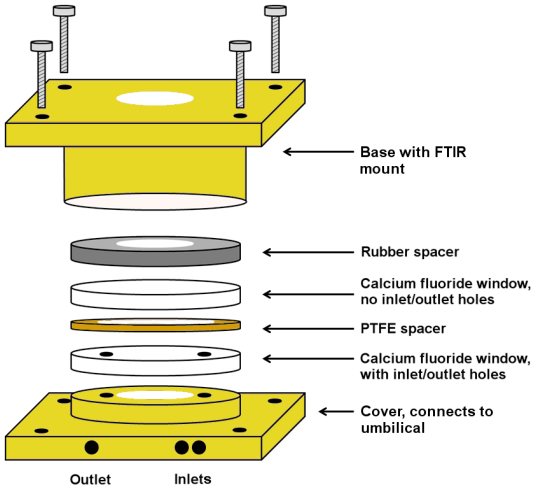

Fig. S2. Schematic of the flow through FTIR observation head for the Biologic SFM 400 stopped flow instrument. The observation head contains two inlet ports, and the final mixing event (mixer 3 in Fig. S1) occurs immediately prior to introduction of solution to the transmission cell.

Reaction of $[Re(bpy\text{-}tBu)(CO)_3]^-$ (1) or $[Re(bpy)(CO)_3]^-$ (2) with CO_2

A comparison of the IR spectrum of Re(bpy-*t*Bu)$(CO)_3$Cl and the product of the stopped-flow reaction between **1** and CO_2 is shown in Fig. S3.

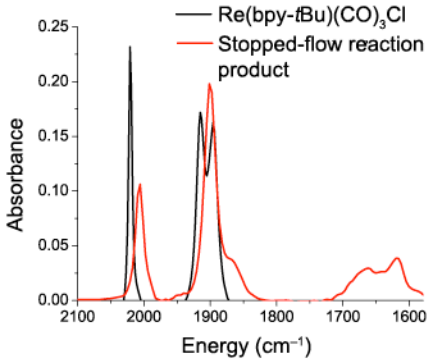

Fig. S3. Comparison of the IR spectra of Re(bpy-*t*Bu)$(CO)_3$Cl (black) and the product from stopped-flow reactions involving **1** and CO_2 (red).

Complex **2** reacts with CO_2, yielding an IR spectrum that indicates the presence of two products (Fig. S4). The ν_{CO} stretches at 2009 and 1901 cm^{-1} are consistent with a Re(I) product which is similar to that observed in the reaction of **1** with CO_2. The ν_{CO} stretches at 1986, 1948, 1886, and 1867 cm^{-1} match precisely with those reported for the $[Re(bpy)(CO)_3]_2$ dimer.[1, 2] For complex **2**, no appreciable formation of intermediates before formation of the fully oxidized species and the Re(0) dimer was observed. This Re(0) dimer has been proposed as a degradation pathway for the Re(bpy)$(CO)_3$Cl family of catalysts.[2] Additionally, the $[Re(bpy)(CO)_3]_2$ dimer could form upon oxidation of anion **2** by the Re(I) product. Dimer formation is not observed as a product of the reactions of **1** with CO_2, suggesting that the *t*Bu groups at the 4,4'-positions of the bpy ligand provide sufficient steric hindrances and/or electronic differences to eliminate this degradation pathway. The presence of this degradation pathway, as well as other factors, helps explain the observed reduced rates of electrocatalysis for **2** as compared to **1**.[3]

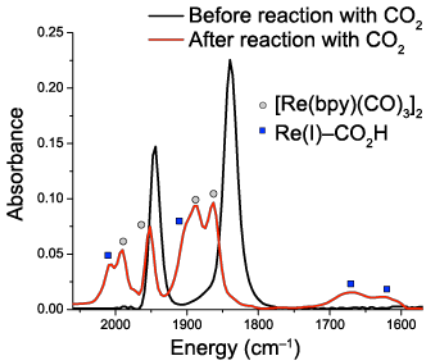

Fig. S4. IR spectra of **2** before reaction with CO_2 (black) and after reaction with CO_2 (red). Grey circles indicate ν_{CO} stretches that correspond to the dimer, $[Re(bpy)(CO)_3]_2$, and blue squares indicate ν_{CO} stretches that correspond to the Re(I)–CO_2H product.

In each reaction, no additional species between the starting anionic complexes and the oxidized products are observed. Therefore, we classify these reactions as fast, net two-electron oxidative additions of CO_2 to the metal centers. It is possible that intermediate species do form, but are fleeting and only accumulate in very small concentrations due to fast conversion to the final state. However, this assignment is supported by experiments with higher concentrations of starting material (15 mM **1** or **2**), which also show no intermediate species.

Isotopic Labeling Experiments

Reactions with $^{13}CO_2$ were performed nearly identically to the reactions with unlabeled CO_2, and the stopped-flow mixing schematic was the same as shown in Fig. S1. However, due to a limited supply of $^{13}CO_2$, it was not possible to sparge THF for a significant amount of time. Nevertheless, we were successful in dissolving *ca.* 80 mM $^{13}CO_2$ in solution (as calculated from the extinction coefficient for CO_2 in the IR, 1300 $M^{-1}cm^{-1}$) (Fig. S5). Here, the $^{13}CO_2$ peak can be seen at 2272 cm^{-1}, as compared to 2333 cm^{-1} for unlabeled CO_2 (a shift of ~61 cm^{-1}).

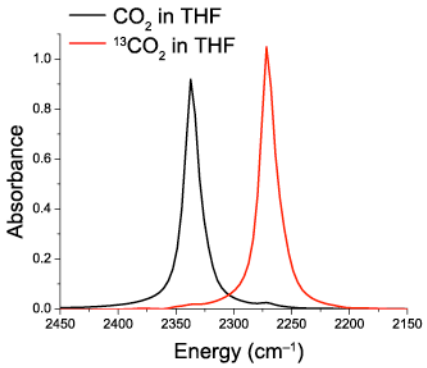

Fig. S5 IR spectra of pure CO_2 in THF (black) and pure $^{13}CO_2$ in THF (red), showing the shift of the CO_2 peak from 2333 cm^{-1} to 2268 cm^{-1}.

Experiments with added H^+

In addition to reactions with added MeOH, we also performed stopped-flow experiments with added H_2O. These experiments were performed in the same manner as experiments with added MeOH, with 2.5 mM **1**, 25 mM CO_2, and *ca.* 0-200 mM H_2O. Very similar reaction kinetics are observed with added H_2O, very much like the experiments with added MeOH. As shown in Fig. S6, with added H_2O, the rate of formation of the stopped-flow reaction product increases significantly. Due to this drastic increase, it is very difficult to distinguish differences in the dependence of these IR frequencies with small differences in pK_a's of various weak Brønsted acids. In this study, we are limited to weak Brønsted acids with a narrow pK_a range because acids with too high of pK_a's will cause Re anions to favor engaging protons over CO_2.

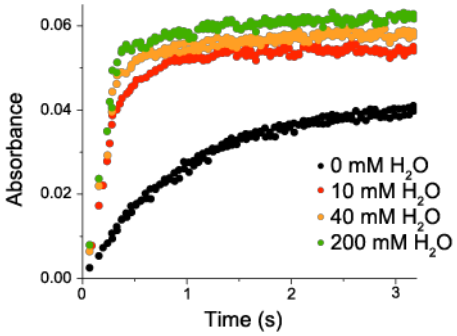

Fig. S6. Growth of the ν_{OCO} stretch at 1616 cm^{-1} as a function of time for the reaction of 2.5 mM **1** with 25 mM CO_2 with the addition of various concentrations of H_2O.

Genuine Re(bpy)(CO)$_3$(CO$_2$H) (2-CO$_2$H)

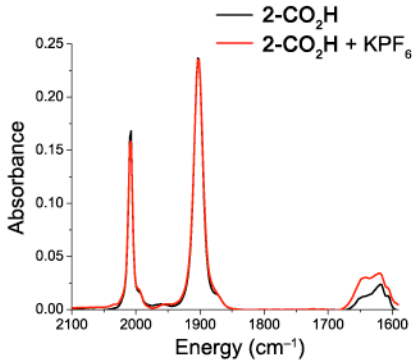

Fig. S7. Comparison of the IR spectra of **2-CO$_2$H** without KPF_6 (black) and with KPF_6 (red). Spectra are normalized relative to each other.

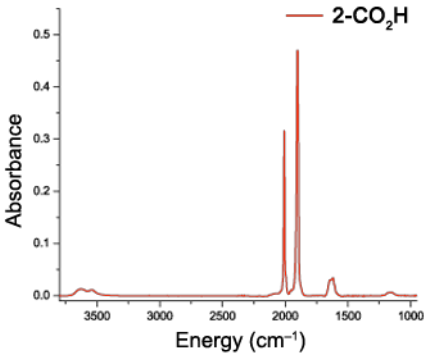

Fig. S8. Full IR spectrum of **2-CO$_2$H** in MeCN from 4000 cm^{-1} to 1000 cm^{-1}.

Table S1. IR stretching frequencies of **1-CO$_2$H** and **2-CO$_2$H** in stopped-flow reactions, synthesized solutions, and gas-phase DFT calculations.

	IR stretching frequencies (cm^{-1})		
Complex	Stopped-flow reaction	Synthesized	DFT-calculated
1-CO$_2$H	2001, 1901, 1662, 1616	–	1992, 1920, 1619
2-CO$_2$H	2009, 1901, 1662, 1616	2008, 1902, 1643, 1617	1997, 1926, 1616

Disproving Carbonate Formation

In order to disprove carbonate (CO_3^{2-}) formation in these stopped-flow experiments, we attempted to take an IR spectrum of a [K(18-crown-6)]$_2$[CO_3] solution in THF. Tetraethylammonium hydroxide was reacted with CO_2, and this solution was placed under vacuum overnight to remove H_2O. KPF_6, 18-crown-6, and THF were added, and the solution was stirred for 10 minutes. The white precipitate was not very soluble in THF, and the IR spectrum of the saturated solution showed no IR features in the range of 2100–1500 cm^{-1}. Therefore, it is unlikely that the ν_{OCO} seen in the stopped-flow experiments (1616 and 1662 cm^{-1}) are from CO_3^{2-}.

Kinetic analysis

3D plots of the stopped-flow reaction of **2** with CO_2 is shown in Fig. S9. Decays of the ν_{CO} stretches at 1940 cm^{-1} for **1** and **2** are shown in Fig. S10. Growths of the ν_{CO} stretches at 1901 cm^{-1} for **1** and **2** are shown in Fig. S11. Growths of the ν_{CO} stretches at 2001 and 2009 cm^{-1} for **1** and **2**, respectively, are shown in Fig. S12. Growths of the ν_{OCO} stretches at 1616 and 1662 cm^{-1} for **1** are shown in Fig. S13. The starting

ν_{CO} stretches at 1940 and 1832 cm^{-1} decay with very similar rates to the growths of the ν_{CO} stretches at 2001 and 1901 cm^{-1} and to the growths of the ν_{OCO} stretches at 1616 and 1662 cm^{-1} (Fig. S14).

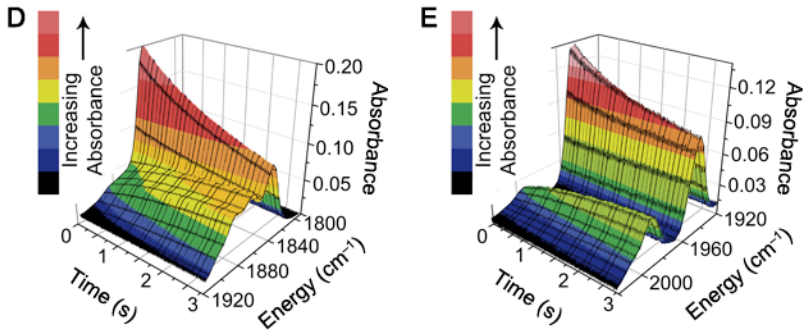

Fig. S9. Reaction of 2.5 mM **2** with 32 mM CO_2: (**A**) 3D plot of the reaction showing the decay of the ν_{CO} stretch at 1840 cm^{-1} and the growth of the ν_{CO} stretch at 1901 cm^{-1}; (**B**) 3D plot of the reaction showing the decay of the ν_{CO} stretch at 1940 cm^{-1} and the growth of the ν_{CO} stretch at 2009 cm^{-1}.

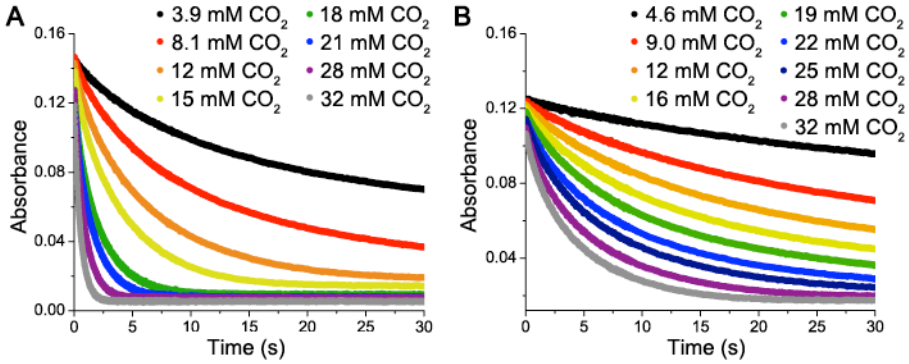

Fig. S10. (**A**) Decays of the ν_{CO} stretch at 1940 cm^{-1} as a function of time for the reaction of 2.5 mM **1** with various concentrations of CO_2. (**B**) Decays of the ν_{CO} stretch at 1940 cm^{-1} as a function of time for the reaction of 2.5 mM **2** with various concentrations of CO_2.

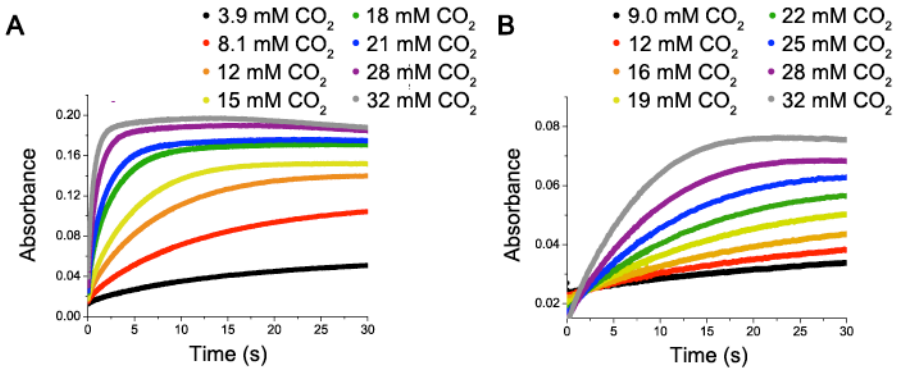

Fig. S11. (**A**) Growths of the ν_{CO} stretch at 1901 cm^{-1} as a function of time for the reaction of 2.5 mM **1** with various concentrations of CO_2. (**B**) Growths of the ν_{CO} stretch at 1901 cm^{-1} as a function of time for the reaction of 2.5 mM **2** with various concentrations of CO_2.

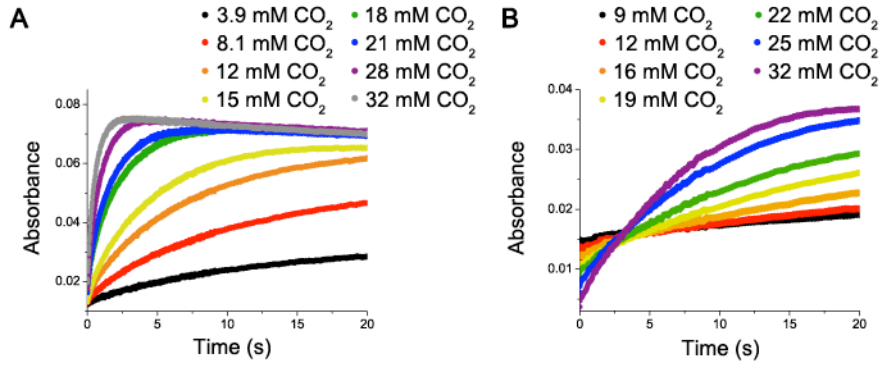

Fig. S12. (**A**) Growths of the ν_{CO} stretch at 2001 cm^{-1} as a function of time for the reaction of 2.5 mM **1** with various concentrations of CO_2. (**B**) Growths of the ν_{CO} stretch at 2009 cm^{-1} as a function of time for the reaction of 2.5 mM **2** with various concentrations of CO_2.

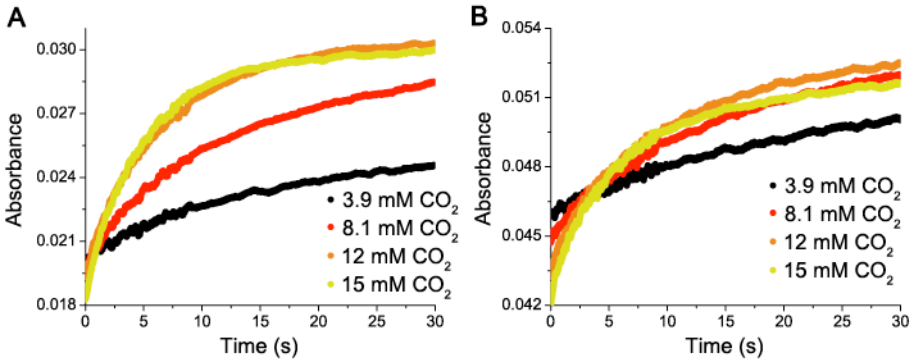

Fig. S13. (**A**) Growths of the ν_{OCO} stretch at 1616 cm^{-1} as a function of time for the reaction of 2.5 mM **1** with various concentrations of CO_2. (**B**) Growths of the ν_{OCO} stretch at 1662 cm^{-1} as a function of time for the reaction of 2.5 mM **1** with various concentrations of CO_2. The growths of these ν_{OCO} stretches saturate around 12 mM CO_2 due to the limited supply of H^+ in solution.

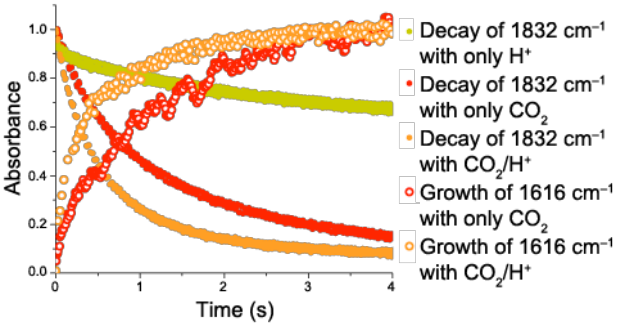

Fig. S14. Comparison of the decay rates of the ν_{CO} stretch at 1832 cm^{-1} and the growth rates of the ν_{OCO} stretch at 1616 cm^{-1} for the reaction of 2.5 mM **1** with various substrates. Data in yellow correspond to reactions with only H^+ added (3 mM MeOH), data in red correspond to reactions with only CO_2 added (25 mM), and data in orange correspond to reactions with both CO_2 and H^+ added (25 mM and 3 mM, respectively). Initial absorbance values for the decays of 1832 cm–1 are normalized to 1 by multiplying each data set by 7.5. Saturated absorbance values for the growths of 1616 cm–1 are normalized to 1 by multiplying each data set by 25.

Pseudo-first order kinetics were fit by plotting the decay of the lowest energy ν_{CO} stretch at 1832 cm^{-1} for **1** and 1840 cm^{-1} for **2** vs. time (Fig. S15 and S16). Pseudo-first order kinetic curves were fit through a minimum of two half-lives for each run at all concentrations of CO_2 studied. Plotting $\ln(A/A_0)$ vs. time gave linear plots through the first two half-lives of the reaction and the slope of the plots gave observed

rates in units of s^{-1} for each complex at each CO_2 concentration (Table S1).[4]

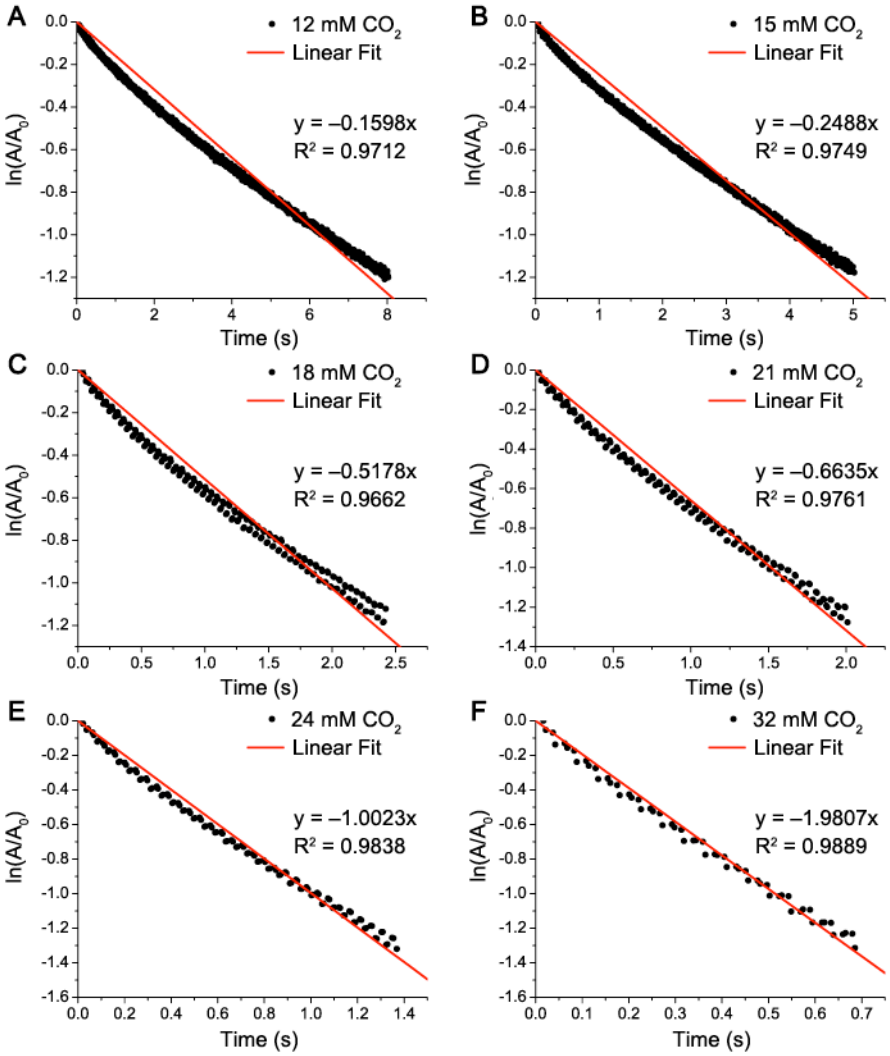

Fig. S15. Plot of $\ln(A/A_0)$ vs. time for the ν_{CO} stretch at 1832 cm^{-1} for the reaction of 2.5 mM **1** with (**A**) 12 mM CO_2, (**B**) 15 mM CO_2, (**C**) 18 mM CO_2, (**D**) 21 mM CO_2, (**E**) 24 mM CO_2, and (**F**) 32 mM CO_2. For each plot, kinetic data is shown in black and a linear fit of the data is shown in red. Similar plots and fits were obtained for the reactions of **1** with 3.9, 8.1, and 28 mM CO_2.

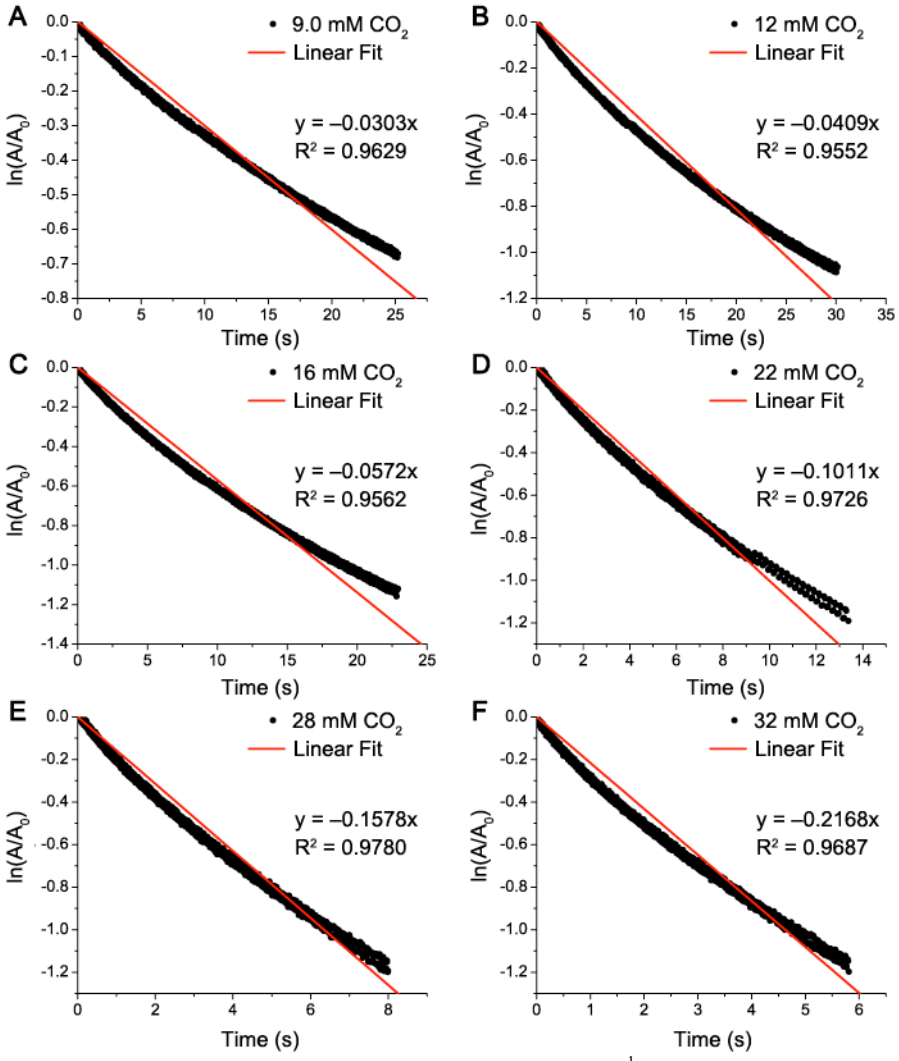

Fig. S16. Plot of ln(A/A$_0$) vs. time for the ν_{CO} stretch at 1840 cm^{-1} for the reaction of 2.5 mM **2** with (**A**) 9.0 mM CO_2, (**B**) 12 mM CO_2, (**C**) 16 mM CO_2, (**D**) 22 mM CO_2, (**E**) 28 mM CO_2, and (**F**) 32 mM CO_2. For each plot, kinetic data are shown in black and a linear fit of the data is shown in red. Similar plots and fits were obtained for the reactions of **2** with 4.6, 19, 25, and 31 mM CO_2.

Table S2. Pseudo-first order rates for the reaction of 2.5 mM **1** and **2** with various concentrations of CO_2 with 18-crown-6 in solution. Rates were obtained by following the decay of the ν_{CO} stretch at 1832 and 1840 cm^{-1} in stopped-flow IR spectroscopy experiments.

[CO_2] (mM)	Rate of **1** (s^{-1})	[CO_2] (mM)	Rate of **2** (s^{-1})
15	0.25	16	0.057
18	0.52	19	0.079
21	0.66	22	0.10
24	1.0	25	0.13
28	2.0	28	0.16
32	2.0	31	0.21

Plots of ln(A/A$_0$) vs. time gave better fits than plotting either 1/[Re] or [Re]$^{1/2}$ vs. time. Second order kinetic analysis was also performed for both complexes at all concentrations of CO_2 studied. This analysis gave the same rates within error as the pseudo-first order fits, but the agreement between the data and the second order kinetic fits was not as suitable as pseudo-first order kinetic fits. As expected, lower concentrations of CO_2 fit second order kinetics slightly better due to a larger change in [CO_2] over the

course of the reaction, while higher concentrations of CO_2 fit pseudo-first order kinetics better. Pseudo-first order kinetic analysis was also completed for the growths of ν_{CO} stretches at 1901 cm^{-1} for complexes **1** and **2**. Rates and half-lives for the growth of these peaks were the same as the decays of ν_{CO} stretches at 1832 and 1840 cm^{-1} (for **1** and **2**, respectively), within experimental error.

We attempted to calculate separate rate constants for the reaction of **2** with CO_2 for the formation of the Re(I) product and for the formation of the dimer, $[Re(bpy)(CO)_3]_2$. For the formation of the Re(I) product, we attempted to fit kinetic data for the growth of the ν_{CO} stretches at 2009 and 1901 cm^{-1}. For the formation of the dimer, we attempted to fit kinetic data for the growth of the ν_{CO} stretches at 1986, 1948, 1886, and 1867 cm^{-1}. However, because most of these ν_{CO} stretches overlap with one another and/or overlap with starting material ν_{CO} stretches, we were unsuccessful in calculating separate rate constants using this analysis.

Plotting pseudo-first order rates (k_{obs}) vs. $[CO_2]$ (for $[CO_2] \geq 15$ mM) gives rise to fairly linear plots and second order rate constants (k_{CO2}) of 120 ± 20 $M^{-1}s^{-1}$ for **1** and 12 ± 1.5 $M^{-1}s^{-1}$ for **2** (Figure S17 and S18). We believe that including only $[CO_2] \geq 15$ mM is justified because we are most interested in comparing the kinetics and mechanisms of these stopped-flow reactions with electrochemical experiments. In electrochemical experiments, we usually have greater than 40-fold excess of CO_2 to the catalyst. Electrochemical reactions are also first order in $[CO_2]$;[5] therefore, the kinetics of these stopped-flow reactions (at high $[CO_2]$ to [Re] ratios) tend to agree well with electrochemical experiments.

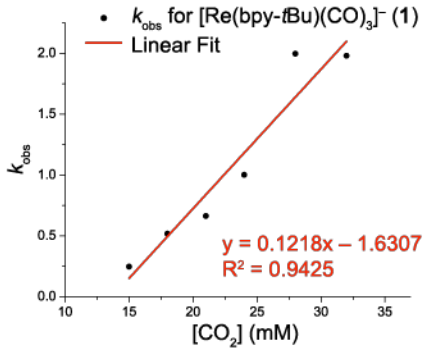

Fig. S17. Plot of k_{obs} vs. $[CO_2]$ for the reaction of 2.5 mM **1** with CO_2. A linear fit of the kinetic data is shown in red (y = 0.1218x – 1.6307). A pseudo-first order rate constant (k_{CO2}) of 120 ± 20 $M^{-1}s^{-1}$ was obtained from this linear fit.

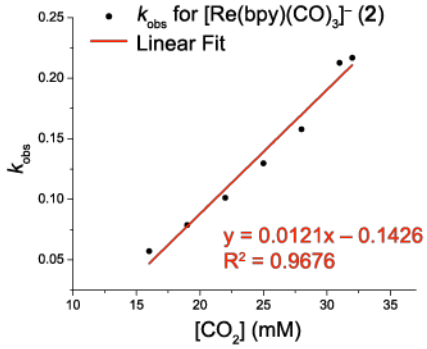

Fig. S18. Plot of k_{obs} vs. $[CO_2]$ for the reaction of 2.5 mM **2** with CO_2. A linear fit of the kinetic data is shown in red (y = 0.0121x – 0.1426). A pseudo-first order rate constant (k_{CO2}) of 12 ± 1.5 $M^{-1}s^{-1}$ was obtained from this linear fit.

Removal of 18-crown-6

Stopped-flow IR spectroscopy experiments were repeated after removing 18-crown-6 that was in solution to form anions **1** and **2**. The IR spectra of **1** and **2** without 18-crown-6 in solution are shown in Fig. S19. The decay of the ν_{CO} stretch at 1832 cm^{-1} for the reaction of **1** with CO_2 without 18-crown-6 in solution is shown in Fig. S20A. Here, this ν_{CO} stretch had almost entirely decayed at the time of the first data point collection, making it impossible to perform detailed kinetic analysis on these reactions. Although we

cannot calculate a rate constant directly through kinetic analysis for the reaction of **1** without 18-crown-6, we can estimate this rate constant at 15,000 $M^{-1}s^{-1}$ by employing both the calculated rate constant for the reaction of **2** without 18-crown-6 (k_{CO2} = 1,500 $M^{-1}s^{-1}$) and the difference in rate constants for the reactions of **1** and **2** with 18-crown-6 in solution (10-fold). This estimation is valid if the reaction of **1** without 18-crown-6 is approximately 10 times faster than the reaction of **2** without 18-crown-6 (as was true for reactions with 18-crown-6 in solution). This estimate of the rate constant is in good agreement with the rate constant in electrocatalysis for **1** (k_{CO2} = 10,000 $M^{-1}s^{-1}$).

For the reaction of **2** without 18-crown-6, decay of the ν_{CO} stretch at 1840 cm^{-1} is observable at low [CO_2] (Fig. S20B), allowing for kinetic analysis. Experiments without 18-crown-6 in solution indicate that reactions are first order in [CO_2]. Fig. S21 shows that a 2-fold increase in [CO_2] results in approximately a 2-fold increase in the observed rate constant (k_{obs}), which is consistent with a first order [CO_2] dependence. Because of this, we are confident that reactions with 18-crown-6 in solution are also first order in [CO_2] at high concentrations of CO_2. Calculated rate constants for reactions of **2** without 18-crown-6 in solution are shown in Table S2.

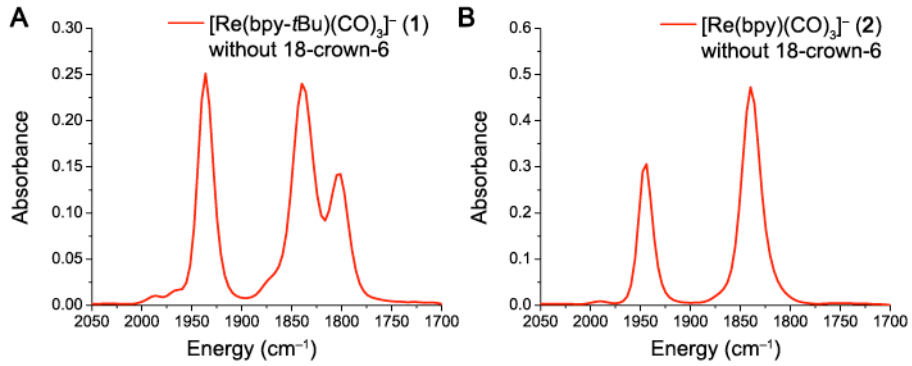

Fig. S19. (**A**) IR spectrum of **1** without 18-crown-6 in solution. (**B**) IR spectrum of **2** without 18-crown-6 in solution. Three ν_{CO} stretches are observed in the spectrum of **1** without 18-crown-6 due to potassium coordination to the carbonyl ligands.

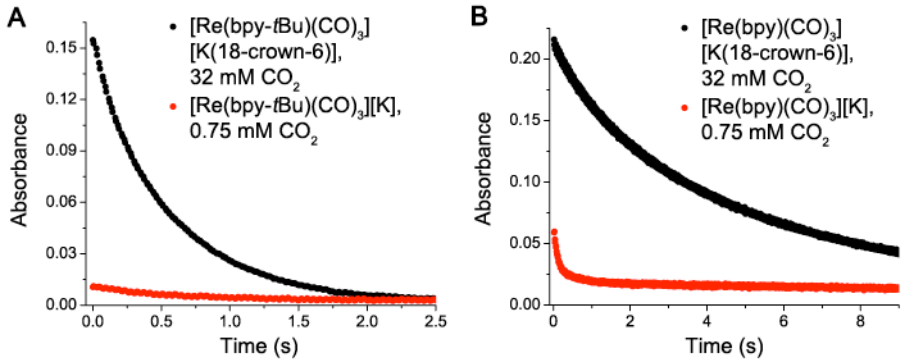

Fig. S20. (**A**) Decay of the ν_{CO} stretch at 1832 cm^{-1} for the reaction of **1** with CO_2 with 18-crown-6 in solution (black, 32 mM CO_2) and without 18-crown-6 in solution (red, 0.75 mM CO_2). (**B**) Decay of the ν_{CO} stretch at 1840 cm^{-1} for the reaction of **2** with CO_2 with 18-crown-6 in solution (black, 32 mM CO_2) and without 18-crown-6 in solution (red, 0.75 mM CO_2).

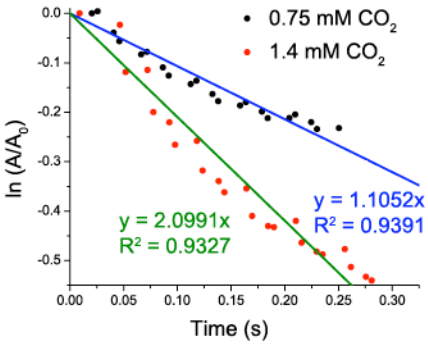

Fig. S21. Plot of $\ln(A/A_0)$ vs. time (ν_{CO} = 1832 cm^{-1}) for the reaction of 2.5 mM **1** with CO_2 without 18-crown-6 in solution. The reaction with 0.75 mM CO_2 is shown in black, with a linear fit of the kinetic data shown in blue. The reaction with 1.4 mM CO_2 is shown in red, with a linear fit of the kinetic data shown in green.

Table S3. Pseudo-first order rates for the reaction of 2.5 mM **2** with various concentrations of CO_2 without 18-crown-6 in solution. Rates were obtained by following the decay of the ν_{CO} stretch at 1840 cm^{-1} in stopped-flow IR spectroscopy experiments.

$[CO_2]$ (mM)	Rate of **2**, no 18-crown-6 (s^{-1})
0.75	1.1
1.4	2.1

Comparison with Previous Stopped-flow UV-Vis Spectroscopy Studies

In previous stopped-flow UV-Vis spectroscopy studies, the reaction of **1** without 18-crown-6 with CO_2-saturated THF was monitored by the decay of the strong absorption at 570 nm.[6] A pseudo-first order rate constant (k_{CO2}) of 350 $M^{-1}s^{-1}$ was calculated for the reaction of 0.06 mM **1** with CO_2. This rate constant is much lower than the rate constant obtained in this study (~15,000 $M^{-1}s^{-1}$). However, the concentration of **1** was significantly smaller in the UV-Vis experiments (0.06 mM) than in these current IR experiments (2.5 mM). Additionally, the UV-Vis experiments involved only one CO_2 concentration (*ca.* 100 mM), while our IR experiments involved a wide range of CO_2 concentrations (*ca.* 1–50 mM). These two factors make it difficult to directly compare the two studies.

In the previous stopped-flow UV-Vis spectroscopy experiments, tetrabutylammonium hexafluorophosphate (TBAH) was added as an electrolyte in solution in order to replicate electrochemical experiments. We added TBAH to solutions of the reduced anions in our stopped-flow IR spectroscopy reactions. However, we did not see any significant difference in reaction rates between these reactions and reactions without TBAH. This indicates that the addition of electrolyte in solution is only useful in an electrochemical manner in order to facilitate electron flow through solution. Since the catalytically-active species are synthetically formed prior to reaction, TBAH does not aid the progression of these stopped-flow reactions. Because we were able to obtain rates for the reaction of **1** with CO_2 that are in reasonable agreement with previous electrocatalysis experiments, we believe this stopped-flow IR spectroscopy study gives much more accurate results than the previously reported stopped-flow UV-Vis spectroscopy study. In addition, stopped-flow IR spectroscopy provides significantly more information about the mechanism and products associated with reactions of anions **1** and **2** with CO_2 than the previous stopped-flow UV-Vis spectroscopy experiments.

Density Functional Theory (DFT) Calculations

In DFT-calculated $Re(bpy)(CO)_3(CO_2H)$, a distinct bipyridine-related stretch occurs at 1453 cm^{-1}, much lower than the observed 1662 and 1616 cm^{-1} of our stopped-flow product. Therefore, the stretches at 1662 and 1616 cm^{-1} are not bipyridine-related. DFT-calculated $[Re(bpy\text{-}R)(CO)_3(CO_2)]^-$ has ν_{OCO} stretches at 1541 and 1535 cm^{-1} for R = *t*Bu and R = H, respectively, and DFT-calculated $[Re(bpy\text{-}R)(CO)_3(CO_2)][K]$ has ν_{OCO} stretches at 1448 and 1470 cm^{-1} for R = *t*Bu and R = H, respectively. This suggests that the

product in our stopped-flow reactions is not $[Re(bpy\text{-}R)(CO)_3(CO_2)]^-$ or $[Re(bpy\text{-}R)(CO)_3(CO_2)][K]$, but rather $Re(bpy)(CO)_3(CO_2H)$. We also used DFT to calculate the interaction of $Re(bpy)(CO)_3(CO_2H)$ with K^+. In the DFT structure of $[Re(bpy)(CO)_3(CO_2H)][K]$, the potassium ion partially coordinates to the CO_2H-adduct and to one or two of the carbonyl ligands (Fig. S24). This causes a 63 cm^{-1} shift for the ν_{OCO} stretch, from 1617 cm^{-1} to 1554 cm^{-1}. Since many orientations between the $Re–CO_2H$ species and K^+ ions are probable in the stopped-flow reactions, this can cause a range of observed ν_{OCO} stretches. We use this reasoning to justify the two observed ν_{OCO} stretches in our stopped-flow product. These two ν_{OCO} stretches could also result from equilibrium between a $Re–CO_2H$ and $Re–CO_2^-$ species.

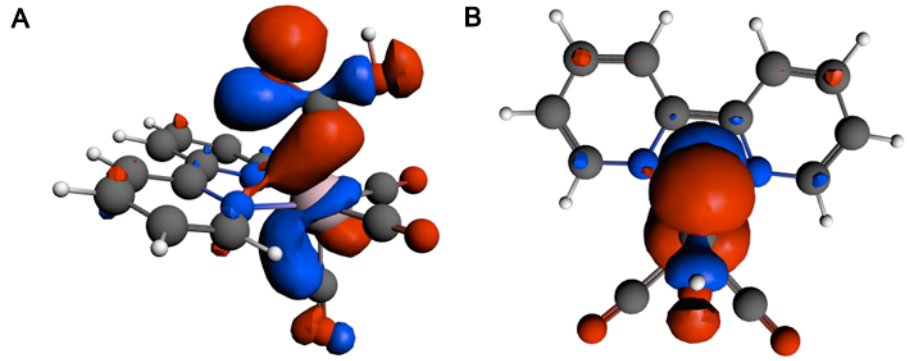

Fig. S22. Side and top view of highest occupied molecular orbital (HOMO) of $Re(bpy)(CO)_3(CO_2H)$ (**2-CO_2H**) calculated with ADF 2012.1

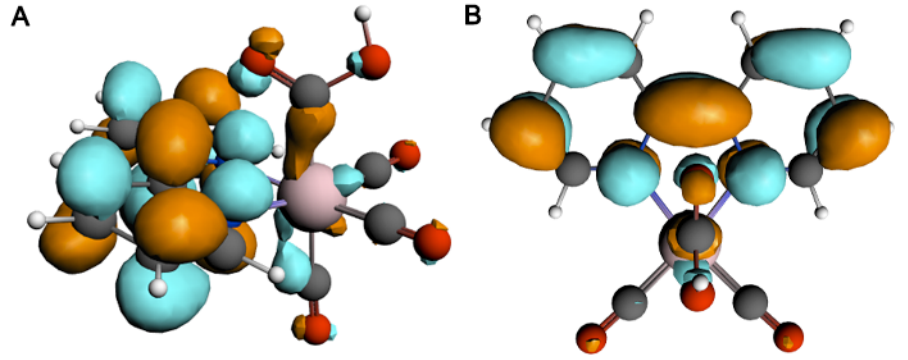

Fig. S23. Side and top view of the lowest unoccupied molecular orbital (LUMO) of $Re(bpy)(CO)_3(CO_2H)$ (**2-CO_2H**) calculated with ADF 2012.1

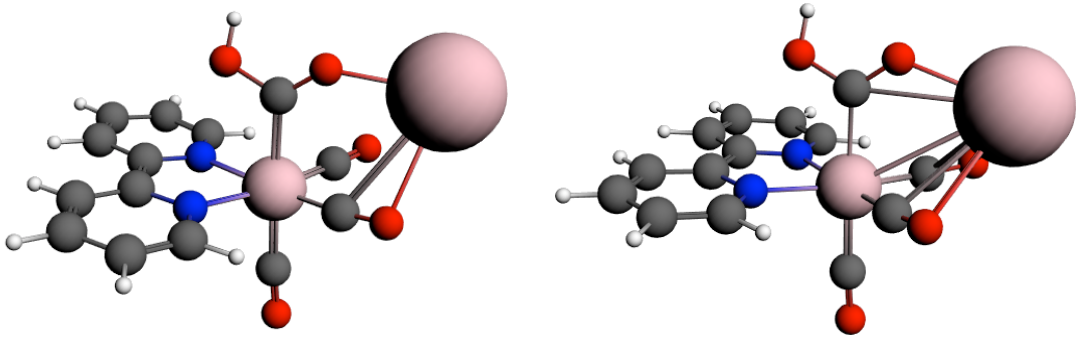

Fig. S24. DFT-calculated structure of $[Re(bpy)(CO)_3(CO_2H)][K]$ showing two different converged structures, calculated with ADF 2012.1

Geometry Optimized xyz Coordinates for Re(bpy)$(CO)_3(CO_2H)$ (2-CO_2H)

Atom	X	Y	Z (Angstrom)
Re	3.026371	1.968157	15.694743
O	5.214482	3.937542	16.664230
O	5.120679	0.162458	14.294824
O	2.720793	3.648001	13.064137
O	2.335121	0.357960	18.243248
O	4.549107	0.492364	17.942706
N	1.386362	2.878925	16.798065
N	1.325443	0.643089	15.396700
C	1.452844	4.071453	17.431245
H	2.366593	4.637977	17.275613
C	0.433364	4.555302	18.235119
H	0.546228	5.521929	18.721678
C	-0.718159	3.780410	18.403438
C	-0.801662	2.560651	17.748780
H	-1.689960	1.944479	17.857742
C	0.261255	2.121637	16.947918
C	0.229933	0.878978	16.175349
C	-0.861738	0.000346	16.169113
H	-1.725116	0.202249	16.797351
C	-0.836882	-1.129368	15.365047
C	0.283730	-1.356465	14.560313
H	0.350610	-2.224485	13.907762
C	1.333648	-0.453699	14.606530
H	2.226289	-0.594446	14.003576
C	4.412462	3.182822	16.284229
C	4.353632	0.861745	14.823473
C	2.790084	3.022446	14.042276
C	3.257121	0.778282	17.551521
H	4.456204	-0.035051	18.768603
H	-1.537354	4.126197	19.032043
H	-1.678002	-1.820802	15.359661

Input File for ADF Calculations of Re(bpy)(CO)$_3$(^{13}CO$_2$H)

```
#$ -S /bin/bash
#$ -cwd

#$ -o output
#$ -e $JOB_ID.err
#$ -j y
#$ -M mdsampso@ucsd.edu
#$ -m beas
#$ -N Rebpy_CO2H_GO
#$ -q all.q
#$ -pe mpi 8

export cur_dir="`pwd`"
echo Running as user `whoami` on `hostname` at `date` in dir `pwd`
export temp_dir="/state/partition1/`whoami`.$JOB_ID"
mkdir $temp_dir
cd $temp_dir
echo With temp dir $temp_dir


# ADF enviroment variables, change as you need

export ADFHOME=/share/apps/adf2012.01/
export ADFBIN=/share/apps/adf2012.01/bin
export ADFRESOURCES=/share/apps/adf2012.01/atomicdata
export SCMLICENSE=/share/apps/adf2012.01/license
export SCM_TMPDIR=$temp_dir
export SCM_USETMPDIR=yes
export NSCM=8
export SCM_IOBUFFERSIZE=512


#Put main code here ****************************************

$ADFBIN/adf -n8 \
<<< "
TITLE Rebpy_CO2H_GO

MAXMEMORYUSAGE 23000

RELATIVISTIC ZORA

UNRESTRICTED

CHARGE 0 0

SCF
DIIS
END

XC
```

```
LDA VWN
GGA Becke Perdew
END

SYMMETRY NOSYM
ATOMS
Re      3.023550    1.972664   15.678732
O       5.205909    3.948885   16.639795
O       5.149021    0.126446   14.386474
O       2.832369    3.573668   12.981966
O       2.362839    0.385186   18.249978
O       4.570673    0.636446   17.988275
N       1.379558    2.869507   16.808030
N       1.316574    0.638507   15.398115
C       1.444131    4.029462   17.493166
H       2.349623    4.612851   17.351042
C       0.437306    4.474449   18.337182
H       0.579329    5.421490   18.851941
C      -0.725085    3.707393   18.517790
C      -0.783280    2.511996   17.799223
H      -1.655735    1.870764   17.894593
C       0.258717    2.107443   16.962035
C       0.212774    0.882774   16.160502
C      -0.898548    0.037491   16.117181
H      -1.763549    0.278206   16.729811
C      -0.926474   -1.096744   15.303049
C       0.228229   -1.330759   14.539418
H       0.308320   -2.189183   13.876732
C       1.304116   -0.458460   14.614557
H       2.200934   -0.629016   14.025468
C       4.405108    3.193887   16.256185
C       4.359964    0.842738   14.858522
C       2.832226    2.987694   13.987638
C.L     3.272851    0.834807   17.561397
H       4.487803    0.127480   18.826692
H      -1.531070    4.025386   19.177479
H      -1.790281   -1.758673   15.262951
END

AtomProps
C.L m=13.0035
END

GEOMETRY
GO
Iterations 200
END

AnalyticalFreq
END

BASIS
type TZ2P
END
```

```
END INPUT
"
# end main code ******************************************

cp * $cur_dir/

# Optional, have to manually clean up otherwise
rm -r -f $temp_dir
```

^{13}C NMR of the reaction of [Re(bpy-*t*Bu)(CO)$_3$]$^-$ (1) with $^{13}CO_2$

In order to further prove the existence of a Re–CO_2H species as a product in the reaction of **1** with CO_2, we utilized ^{13}C NMR spectroscopy. The reaction of anion **1** with $^{13}CO_2$ in THF-d_8 results in a ^{13}C NMR spectrum with peaks at 161.61 and 168.25 ppm, in addition to peaks for the bipyridine carbons and carbonyl ligands (Fig. S26). We believe that the peak at 161.61 ppm corresponds to the –CO_2H group in the reaction product. The peak at 168.25 ppm could result from either bicarbonate (HCO_3^-) or degradation of the Re–CO_2H species into a μ_2-η^2-CO_2-bridged complex, fac, fac-Re(bpy-*t*Bu)(CO)$_3$(CO_2)Re(bpy-*t*Bu)(CO)$_3$ (as seen in similar studies by Gibson).[7] Bicarbonate could be formed in a variety of degradation reactions, such as by degradation of the Re–CO_2H species to [Re(bpy-*t*Bu)(CO)$_4$]$^+$and OH^- which can rapidly react with the excess CO_2. For comparison, Fig. S26 shows the ^{13}C NMR spectrum of $KHCO_3$ in a mixture of THF-d_8/H_2O, and a similar peak at 168.91 ppm is observed.

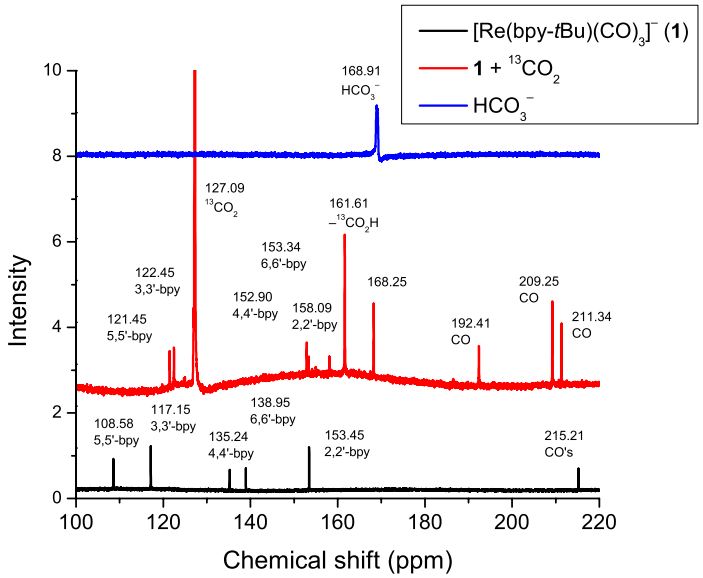

Fig. S25. ^{13}C NMR spectra (from 100–220 ppm) for the reaction between [Re(bpy-*t*Bu)(CO)$_3$]$^-$ (**1**) and $^{13}CO_2$ in THF-d_8, mimicking stopped-flow reactions. The starting anionic complex **1** is shown in black and the reaction product between **1** and $^{13}CO_2$ is shown in red. The ^{13}C NMR spectrum of bicarbonate (HCO_3^-) in a THF-d_8/H_2O mixture is shown in blue for comparison purposes. The assignments for the ^{13}C NMR chemical shifts are shown in the figure.

References

1 F. P. A. Johnson, M. W. George, F. Hartl and J. J. Turner, *Organometallics*, 1996, **15**, 3374.
2 E. E. Benson and C. P. Kubiak, *Chem. Commun.*, 2012, **48**, 7374.
3 J. M. Smieja and C. P. Kubiak, *Inorg. Chem.*, 2010, **49**, 9283.
4 K. A. Connors, *Chemical kinetics, the study of reaction rates in solution*, Wiley-VCH Publishers, Weinheim, Germany, 1991.
5 K.-Y. Wong, W.-H. Chung and C.-P. Lau, *J. Electroanal. Chem.*, 1998, **453**, 161.

6 J. M. Smieja, E. E. Benson, B. Kumar, K. A. Grice, C. S. Seu, A. J. M. Miller, J. M. Mayer and C. P. Kubiak, *Proc. Nat. Acad. Sci., USA*, 2012, **109**, 15646.
7 D. H. Gibson and X. Yin, *J. Am. Chem. Soc.*, 1998, **120**, 11200.